SkinMamba: A Precision Skin Lesion Segmentation Architecture with Cross-Scale Global State Modeling and Frequency Boundary Guidance

Paper ID #3

Shun Zou[1][*], Mingya Zhang[2][*], Bingjian Fan[1], Zhengyi Zhou[1], and Xiuguo Zou[1][†]

[1] College of Artificial Intelligence, Nanjing Agricultural University
{zs,fbj,19222120}@stu.njau.edu.cn, zouxiuguo@njau.edu.cn
[2] State Key Laboratory for Novel Software Technology, Nanjing University
dg20330034@smail.nju.edu.cn

Abstract. Skin lesion segmentation is a crucial method for identifying early skin cancer. In recent years, both convolutional neural network (CNN) and Transformer-based methods have been widely applied. Moreover, combining CNN and Transformer effectively integrates global and local relationships, but remains limited by the quadratic complexity of Transformer. To address this, we propose a hybrid architecture based on Mamba and CNN, called SkinMamba. It maintains linear complexity while offering powerful long-range dependency modeling and local feature extraction capabilities. Specifically, we introduce the Scale Residual State Space Block (SRSSB), which captures global contextual relationships and cross-scale information exchange at a macro level, enabling expert communication in a global state. This effectively addresses challenges in skin lesion segmentation related to varying lesion sizes and inconspicuous target areas. Additionally, to mitigate boundary blurring and information loss during model downsampling, we introduce the Frequency Boundary Guided Module (FBGM), providing sufficient boundary priors to guide precise boundary segmentation, while also using the retained information to assist the decoder in the decoding process. Finally, we conducted comparative and ablation experiments on two public lesion segmentation datasets (ISIC2017 and ISIC2018), and the results demonstrate the strong competitiveness of SkinMamba in skin lesion segmentation tasks. The code is available at https://github.com/zs1314/SkinMamba.

Keywords: Skin lesion segmentation · Mamba · Frequency boundary guidance · CNN

---

[1] [*] These authors contributed equally to this work.

[2] [†] Corresponding author.

1   Introduction

According to the 2023 global cancer statistics [41], tens of thousands of people die annually from malignant skin lesions, with melanoma, a highly lethal skin cancer, becoming one of the fastest-growing cancers worldwide. In recent years, the advancement of computer technology has led to the widespread use of computer-aided diagnosis (CAD) in the medical field [5, 20, 25, 43]. Automated skin lesion segmentation systems assist medical professionals in rapidly and accurately identifying lesion areas. In medical image segmentation, we mainly use Convolutional Neural Networks (CNN) [3] and Vision Transformers (ViT) [48, 52, 61]. However, both have certain limitations. CNN excels at capturing local features but fails to fully extract global features, which reduces segmentation accuracy. ViT captures long-range dependencies, enabling efficient global modeling and focusing on key areas of the image, but its quadratic complexity results in a high computational burden. Although some studies have attempted to explore efficient attention mechanisms [29, 44, 45, 47] or combine CNNs with ViTs to create lightweight hybrid models [27, 35, 56], these approaches often come at the cost of reducing the ability to capture global features. The trade-off between efficient global modeling and computational efficiency remains unresolved.

In recent years, State Space Models (SSM) [13, 19, 24] have attracted the attention of many researchers. S4 [15] initially applied SSM to the deep learning field, but its performance still lagged behind CNN and Transformer. Thanks to Mamba [11], which enhances SSM through an efficient selective scanning mechanism, it not only establishes long-range dependencies but also demonstrates linear complexity related to input size. Inspired by Mamba, Vision Mamba [63] and Visual Mamba [28] were the first to introduce Mamba into the visual domain, achieving remarkable results. Additionally, numerous researchers have applied it to medical image segmentation, such as VM-UNet [37], U-Mamba [31], OC-TAMamba [65], and H-vmunet [50]. However, challenges remain in skin lesion segmentation. For instance, the boundaries of the lesion areas are unclear, the sizes of the lesion regions vary, and there is significant information loss during downsampling. Additionally, we observed that directly applying Mamba to lesion segmentation results in reduced accuracy due to the inability to capture local fine-grained features.

To address the aforementioned issues, we propose SkinMamba, which combines the advantages of Mamba in learning global features and CNN in extracting local features. Specifically, the overall architecture follows a 5-level encoder-decoder structure. The core components of the model are the Scale Residual State Space Block (SRSSB) and the Frequency Boundary Guided Module (FBGM). In SRSSB, we introduce the Visual State Space Block (VSSB) to achieve efficient global modeling, while the Scale-Mixed Feed-Forward Layer (SMFFL) is used to extract cross-scale features, promoting the interaction of multi-level information and enabling multi-scale, multi-level feature representation in a global context. To mitigate the loss of boundary information caused by downsampling, we introduce the Frequency Boundary Guided Module (FBGM), which captures boundary cues from a frequency perspective and guides the de-

coder during the decoding process. Through this design, we developed the Skin-Mamba model, which maintains computational efficiency while effectively capturing both short- and long-range dependencies. It also addresses challenges such as unclear boundaries and varying lesion sizes in lesion images, further exploring Mamba's application in skin lesion segmentation.

The main contributions of our work are as follows:

- We proposed SkinMamba, a hybrid architecture based on Mamba and CNN, effectively combining the strengths of both. By addressing challenges such as varying lesion sizes and blurred boundary information in lesion segmentation, we further optimized the model architecture and explored the application of Mamba in this task.
- We introduced the Scale Residual State Space Block (SRSSB) to facilitate expert knowledge exchange across different levels in a global state and incorporated the Frequency Boundary Guided Module (FBGM) to achieve high-frequency restoration and boundary prior guidance.
- Extensive experiments on two open-source lesion segmentation datasets demonstrated that SkinMamba outperformed state-of-the-art methods in terms of mIoU, DSC, Acc, Spe, and Sen.

2   Related Work

2.1   Medical Image Segmentation

FCN [30] uses fully convolutional layers to extract image features, becoming a pioneer in image segmentation. However, medical image segmentation requires more detailed lesion feature learning compared to natural scene segmentation. Scale variation is a critical issue in medical image segmentation. UNet [36] addressed this by proposing an encoder-decoder architecture that effectively integrates low-level and high-level features, making it a cornerstone in medical image segmentation.

Since the introduction of UNet, many researchers have proposed variants to improve upon it. UNet++ [62] replaces the traditional cropping and concatenation operations with dense convolutions, achieving tighter feature fusion in skip connections and reducing the impact of information loss during sampling. Attention-UNet [33] integrates attention mechanisms into the UNet framework, focusing more on target regions and suppressing irrelevant information. To reduce information loss and improve overall performance, Res-UNet [53] introduces Res-blocks to enhance feature transfer stability and training of deep networks. Dense-UNet [17] utilizes Dense-blocks for efficient feature reuse, improving multi-scale information capture. U-Net v2 [34] employs an innovative skip connection mechanism to mix high-level and low-level features, achieving refined feature fusion and enhancing the integration of features across different scales.

However, models using only CNNs suffer from reduced performance due to their inability to capture global features. To address this, researchers introduced Transformers from natural language processing (NLP) to computer vision [46],

developing Vision Transformer (ViT) for efficient global modeling. In medical image segmentation, TransUNet [7] was the first to integrate ViT's feature learning capabilities into the U-Net encoder. By combining ViT's self-attention mechanism with U-Net's structural advantages, TransUNet improved feature representation accuracy and the model's understanding of complex image content. Swin-UNet [4] incorporates Swin Transformer network modules into the U-Net structure, enhancing feature learning capabilities. Attention Swin U-Net [1] operates with a cascaded attention mechanism and optimizes Swin-UNet. This cascading attention mechanism allows the model to more precisely capture and fuse important information during feature processing. Although Transformers excel in global modeling, their attention mechanism faces high quadratic complexity in long sequence modeling, resulting in significant computational burden [46]. This is a considerable issue, especially for dense prediction tasks such as medical image segmentation.

2.2   State Space Models (SSMs)

In recent years, State Space Models (SSMs) [16, 24] have gained attention in deep learning, particularly in dynamic system modeling. These models originated from state-space theory in control systems and have shown potential in capturing complex temporal dependencies. To address the issue of long-range dependencies that traditional temporal models struggle with, researchers have improved SSMs. For instance, S4 [15] uses a normalized diagonal matrix structure to reduce computational complexity, making it an effective alternative to CNNs and Transformers. Subsequent work, such as S5 [42], introduced a MIMO structure and optimized the performance of S4 layers through parallel scanning, proposing a new S5 layer. The Gated State Space layer further enhances model expressiveness by incorporating additional gating units in the S4 layer [32]. Recently, Mamba [28] has significantly improved the processing capability of SSMs for long-sequence tasks by introducing input-based dynamic parameter adjustments and utilizing highly optimized hardware algorithms. This advancement not only simplifies the model structure but also effectively addresses efficiency issues in processing long-sequence data, particularly in fields such as language and genomics.

Following the success of Mamba, researchers have studied this framework in various fields, including image classification [14,31,55,66], low-level [8,18,40,60], point cloud analysis [26,58], and remote sensing images [6,59,64], making it a strong competitor to both CNNs and Transformers. In recent work, Mamba-based vision backbones have been applied to medical image segmentation. VM-UNet [37] introduced the Visual State Space (VSS) module as a foundational block to build an asymmetric encoder-decoder structure, capturing extensive contextual information. U-Mamba [31] and SegMamba [54] incorporated the SSM-Conv hybrid module, effectively leveraging the strengths of CNNs in local feature extraction and Mamba in long-range modeling. T-Mamba [21] integrated shared positional encoding and frequency-based feature fusion into Vision
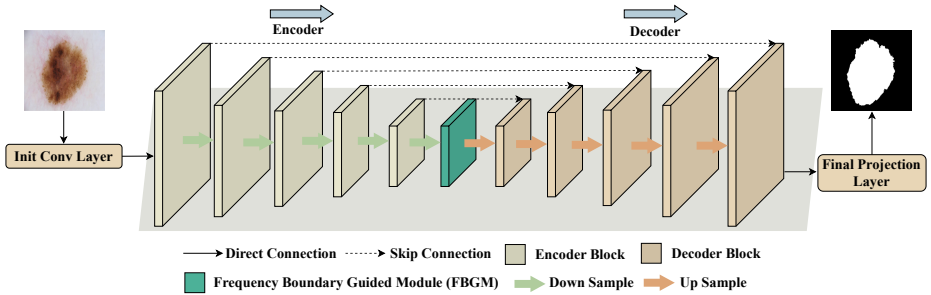
Fig. 1: The illustration of SkinMamba architecture.

Mamba to address limitations in frequency-domain spatial retention and feature enhancement.

In this paper, we will further explore the application of the Visual State Space Model (VSSM) in skin lesion segmentation, thoroughly examining the limitations of Mamba in this task and addressing the remaining challenges in skin lesion segmentation, to optimize the model architecture accordingly.

3 Method

In this section, we first describe the entire pipeline, followed by details of the Encoder and Decoder Blocks. Finally, we elaborate on the two core components: the Scale Residual State Space Block (SRSSB) and the Frequency Boundary Guided Module (FBGM).

3.1 Architecture Overview

Our proposed SkinMamba is shown in Fig. 1. It includes an Init Conv Layer, an Encoder, an FBGM, a Decoder, a Final Projection Layer, and skip connections. Given an input image $x \in \mathbb{R}^{H \times W \times 3}$, the Init Conv Layer first maps the channels of x to C, with C defaulting to 16. Then, the Encoder performs deep feature extraction. Specifically, the Encoder consists of five stages, each comprising an Encoder Block and a downsampling layer. After passing through each stage, the input is mapped to a deeper feature space, while the image width and height are halved, and the number of channels is doubled. Similarly, the Decoder consists of five stages. Each stage includes a Decoder Block and an upsampling layer, where the image width and height are doubled, and the number of channels is halved. Notably, between the Encoder and Decoder, we introduce the FBGM to extract precise boundary cues from a frequency perspective, providing strong constraints for skin lesion segmentation and guiding image decoding. After the Decoder, the Final Projection Layer restores the channel count to match the segmentation target. For skip connections, we use simple addition operations to avoid unnecessary parameters, making it easier to validate the effectiveness of our architecture.
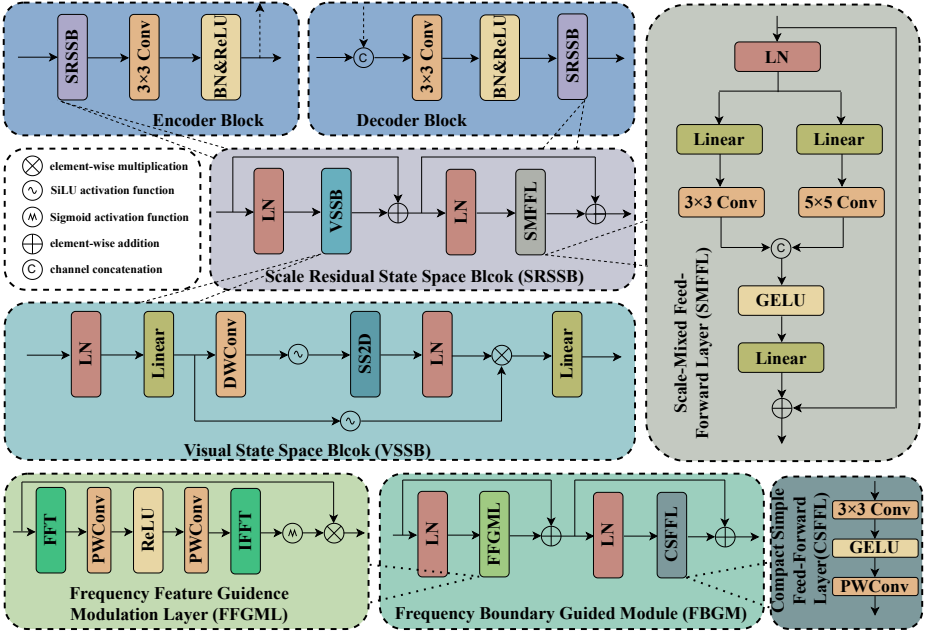
Fig. 2: Key Components of SkinMamba.

3.2 Encoder and Decoder Blcoks

Fusion and balance are the central themes of our architecture. Both the Encoder and Decoder blocks consist of CNN and SRSSB, combining Mamba's strength in learning global features with CNN's ability to extract local features.

As shown in Fig. 2, in the Encoder block, the input features first pass through the SRSSB, followed by a 3×3 convolution, batch normalization (BN) layer, and ReLU activation function, producing the output features that are also used for skip connections. In the Decoder block, each Decoder block receives features from the FBGM or the previous Decoder block, along with the corresponding output features from the Encoder block's skip connections. These two sets of features are then aggregated along the channel dimension to form the fused features. The fused features pass through a 3×3 convolution, BN layer, and ReLU activation function, and finally, the features are fed into the SRSSB.

3.3 Scale Residual State Space Blcok

The SRSSB is used to extract cross-scale mixed information from the global stream and to model long-range dependencies. As shown in Fig. 2, the core components of SRSSB are the Visual State Space Block (VSSB) and the Scale-Mixed Feed-Forward Layer (SMFFL). Specifically, it is divided into two stages. In the first stage, the input features are first passed through a Layer Normalization

(LN) layer, followed by the VSSB to model global information. The second stage takes the features from the first stage, applies layer normalization to prevent mode collapse, and then processes them through the SMFFL to extract multi-scale features. This results in scale features under a global context, while residual connections help maintain consistent information flow across the SRSSB blocks, accelerating model convergence. The above process is defined as follows:

$$X_l' = X_{l-1} + VSSB(LN(X_{l-1})) \tag{1}$$

$$X_l = X_l' + SMFFL(LN(X_l')) \tag{2}$$

Here, $LN(\cdot)$ denotes the layer normalization operation, X_{l-1} represents the input features, while X_l' and X_l are the output features from the VSSB and SMFFL, respectively.

Visual State Space Block. Fig. 2 illustrates the VSSB. The input features X undergo layer normalization and a linear layer, generating two information streams. This process can be represented as:

$$F_1 = F_2 = Linear(LN(X)) \tag{3}$$

Where $Linear(\cdot)$ represents processing through a linear layer, F_1 and F_2 are the inputs for the first and second information streams, respectively. In the first stream, the input features F_1 are processed by depth-wise separable convolution (DWConv) and the SiLU activation function, where preliminary features are extracted. These features are then refined through the 2D selective scanning (SS2D) module and normalized to produce the refined features F_1'. In the second stream, the input features F_2 are processed by the SiLU activation function, where supplementary features F_2' are generated. The refined and supplementary features are then element-wise multiplied, merged, and passed through a linear layer to produce the final output of the VSSB, achieving comprehensive feature representation through detailed extraction and efficient global modeling. The above process is defined as follows:

$$F_1' = LN(SS2D(SiLU(DW(F_1)))) \tag{4}$$

$$F_2' = SiLU(F_2) \tag{5}$$

$$F_{VSSB} = Linear(F_1' \otimes F_2') \tag{6}$$

Where $DW(\cdot)$ denotes depth-wise separable convolution, $SiLU(\cdot)$ represents the SiLU activation function, $SS2D(\cdot)$ indicates 2D selective scanning, $\otimes$ signifies element-wise multiplication, and F_{VSSB} denotes the final output features of the VSSB.

Scale-Mixed Feed-Forward Layer. As shown in Fig. 2, the SMFFL is a dual-branch multi-scale architecture. Specifically, the input features Map undergo layer normalization and are then divided into two branches. Each branch

consists of a linear layer and a 3×3 or 5×5 convolution. First, the features are mapped to a low-dimensional space through the linear layer, and then different sizes of convolutions are used to capture features from the low-dimensional hidden layer. Subsequently, the low-dimensional features at different scales are aggregated along the channel to obtain scale-mixed features. Finally, GELU is applied for non-linear transformation, and a linear layer is used to remap the features back to the original high dimension, while the residual features are added to the scale-mixed features to facilitate gradient flow and propagation. The entire computational process of the module is defined as follows:

$$Map^{'} = LN(Map) \tag{7}$$

$$Map_1 = f^{3\times3}(Linear(Map^{'})) \tag{8}$$

$$Map_2 = f^{5\times5}(Linear(Map^{'})) \tag{9}$$

$$Map_{residual} = Map \tag{10}$$

$$Map_{SMFFL} = Linear(GELU([Map_1, Map_2])) \oplus Map_{residual} \tag{11}$$

Where $f^{x\times y}(\cdot)$ represents the $X \times Y$ standard convolution operation, $[\cdot, \cdot]$ denotes the concatenation operation, $GELU(\cdot)$ represents the GELU activation function, and $\oplus$ signifies element-wise addition. Additionally, we can observe that while the VSSB does not require positional encoding, the SMFFL plays a crucial role in promoting the interaction of multi-scale information flows. The SMFFL enhances synchronized operations, enabling each dimension and scale to contribute its specialized knowledge, thereby achieving precise and complementary detail extraction.

3.4   Frequency Boundary Guided Module

Generally, low-frequency information contains positional relationships and spatial information, while high-frequency information primarily includes specific boundary details. However, most methods reduce image resolution during encoding through downsampling to alleviate computational load. In such cases, decoding relies solely on the low-resolution image, leading to performance degradation and loss of high-frequency information. High-frequency information is crucial for the accurate segmentation of lesion areas on the skin. To address this, we developed the FBGM from a frequency perspective to provide sufficient boundary priors, accurately extract boundary clues, and guide the decoding process. As shown in Fig. 2, the Frequency Feature Guidance Modulation Layer (FFGML) and the Compact Simple Feed-Forward Layer (CSFFL) are the core components of FBGM. Given the input features K_{l-1}, the proposed FBGM can be expressed as follows:

$$K_l^{'} = K_{l-1} + FFGML(LN(K_{l-1})) \tag{12}$$

$$K_l = K_l^{'} + CSFFL(LN(K_l^{'})) \tag{13}$$

Where $K_l^{'}$ and K_l represent the output features of the FFGML and CSFFL, respectively.

Frequency Feature Guidance Modulation Layer. Fig. 2 illustrates the FFGML. Specifically, given the input features F_0, they are transformed into the frequency domain using Fast Fourier Transform (FFT). We then process these frequency domain features with two layers of pointwise convolution (PWConv), interspersed with a ReLU activation function. Finally, the processed features are converted back to the original spatial domain using Inverse FFT, followed by a secondary modulation with the Sigmoid activation function. This modulated output interacts with the input features to obtain the updated feature representation of the original latent layer's hidden space. The above process is defined as follows:

$$F_{mod} = \vartheta^{-1}(PW(ReLU(PW(\vartheta(F_0))))) \tag{14}$$

$$\hat{F}_{mod} = Sigmoid(F_{mod}) \tag{15}$$

$$F_{FFGML} = \hat{F}_{mod} \otimes F_0 \tag{16}$$

Where $\vartheta(\cdot)$ denotes FFT, $\vartheta^{-1}(\cdot)$ represents Inverse FFT, $PW(\cdot)$ denotes pointwise convolution, and $Sigmoid(\cdot)$ represents the Sigmoid activation function.

Compact Simple Feed-Forward Layer. Inspired by the Vision Transformer (ViT) [12], we designed a Compact Simple Feed-Forward Layer (CSFFL) for nonlinear transformation and dimensionality reduction. Given the input features X, we first apply a 3×3 convolution to increase the dimensionality, enhancing both the number of channels and local feature representation. This is followed by the introduction of nonlinearity through the GELU activation function. Finally, a PWConv is used to restore the original number of channels. The entire module is defined as follows:

$$X^{'} = PW(GELU(f^{3\times3}(X))) \tag{17}$$

4 Experiments

4.1 Datasets

In this section, we conducted extensive experiments on two public lesion segmentation datasets: the International Skin Imaging Collaboration 2017 and 2018 challenge datasets (ISIC2017 and ISIC2018), to train and evaluate the proposed model [9, 10]. ISIC2017 and ISIC2018 contain 2,150 and 2,694 dermoscopic images with segmentation mask labels, respectively. Following previous studies [38, 39], we split the datasets into training and test sets at a 7:3 ratio. Specifically, the ISIC2017 training set consists of 1,500 images, while the test set contains 650 images. The ISIC2018 training set consists of 1,886 images, while the test set contains 808 images.

Table 1: Comparative experimental results on the ISIC2017 dataset. The best results are highlighted in bold fonts. " ↑ "and " ↓ " indicate that larger or smaller is better.

Model	Year	mIoU(%)↑	DSC(%)↑	Acc(%)↑	Spe(%)↑	Sen(%)↑
UNet [36]	2015	75.97	86.34	95.53	97.75	84.47
R2UNet [2]	2018	73.43	84.68	95.08	97.86	81.25
UNet++ [62]	2019	77.85	87.55	95.91	97.94	85.82
R2AttUNet [67]	2021	75.07	85.76	95.24	97.17	85.63
SwinUnet [1]	2022	67.93	80.90	93.75	96.69	79.11
MISSFormer [23]	2022	75.84	86.26	95.62	**98.34**	82.09
MALUNet [38]	2022	74.69	85.51	95.15	97.10	85.46
H2Former [22]	2023	76.27	86.54	95.58	97.72	84.90
EGE-UNet [39]	2023	76.50	86.68	95.65	97.88	84.55
MHorunet [49]	2024	78.16	87.73	95.77	97.15	85.99
VMUNet [37]	2024	77.24	87.16	95.78	97.82	85.62
VMUNet v2 [57]	2024	75.25	85.88	95.34	97.47	84.71
H-vmunet [50]	2024	78.18	87.75	95.82	97.12	85.72
ULVM-UNet [51]	2024	78.13	87.72	95.78	97.59	83.61
SkinMamba	-	**78.30**	**87.83**	**96.00**	97.99	**86.14**

Table 2: Comparative experimental results on the ISIC2018 dataset. The best results are highlighted in bold fonts. " ↑ "and " ↓ " indicate that larger or smaller is better.

Model	Year	mIoU(%)↑	DSC(%)↑	Acc(%)↑	Spe(%)↑	Sen(%)↑
UNet [36]	2015	77.22	87.15	93.86	96.56	85.47
R2UNet [2]	2018	71.74	83.55	92.36	96.41	79.74
UNet++ [62]	2019	79.14	88.36	94.40	96.69	87.28
R2AttUNet [67]	2021	75.24	85.87	93.15	95.62	85.47
SwinUnet [1]	2022	74.26	85.23	92.87	95.55	84.54
MISSFormer [23]	2022	77.94	87.60	94.11	96.89	85.48
MALUNet [38]	2022	78.09	87.70	94.07	96.41	86.80
H2Former [22]	2023	77.33	87.21	93.89	96.57	85.56
EGE-UNet [39]	2023	78.90	88.20	94.25	96.17	88.29
MHorunet [49]	2024	79.40	88.52	94.47	96.70	87.55
VMUNet [37]	2024	74.14	85.15	93.03	96.54	82.10
VMUNet v2 [57]	2024	78.25	87.80	94.09	96.25	87.38
H-vmunet [50]	2024	79.41	88.52	94.37	96.03	89.20
ULVM-UNet [51]	2024	78.74	88.10	94.29	96.68	86.85
SkinMamba	-	**80.65**	**89.29**	**94.73**	**97.24**	**90.18**

Table 3: Ablation study on VSSB.

Setting	mIoU(%)↑	DSC(%)↑	Acc(%)↑	Spe(%)↑	Sen(%)↑
Ours	80.65	89.29	94.73	97.24	90.18
Conv	77.56	87.36	93.88	96.12	86.93
self-attention	78.25	87.81	94.06	96.31	87.62

4.2   Implementation Details

We implemented our SkinMamba using PyTorch 2.0.0 and trained it on an NVIDIA RTX 3090 with 24 GB of memory for 300 epochs with a batch size of 32. The input images are uniformly resized to 224×224. We employed data augmentation techniques such as random flipping and random rotation to prevent overfitting. We used the AdamW optimizer with an initial learning rate of 1×10^{-3}, β_1 of 0.9, β_2 of 0.999, and weight decay of 1×10^{-4}. Additionally, we applied a cosine annealing learning rate decay strategy and an early stopping mechanism. To ensure reproducibility, we set the random seed to 42.

4.3   Evaluation Metrics

We used five metrics to evaluate the segmentation performance: Mean Intersection over Union (mIoU), Dice Similarity Score (DSC), Accuracy (Acc), Sensitivity (Sen), and Specificity (Spe). The mathematical formulations for these metrics are summarized as follows:

$$mIoU = \frac{TP}{TP + FP + FN} \tag{18}$$

$$DSC = \frac{2TP}{2TP + FP + FN} \tag{19}$$

$$Acc = \frac{TP + TN}{TP + TN + FP + FN} \tag{20}$$

$$Sen = \frac{TP}{TP + FN} \tag{21}$$

$$Spe = \frac{TN}{TN + FP} \tag{22}$$

Where TP, FP, FN, TN represent true positive, false positive, false negative, and true negative.

4.4   Comparison Results

To validate the effectiveness of our approach, we compared SkinMamba with other state-of-the-art methods. Specifically, this comparison includes UNet [36], R2UNet [2], UNet++ [62], R2AttUNet [67], SwinUnet [1], MISSFormer [23], MALUNet [38], H2Former [22], EGEUNet [39], MHorunet [49], VMUNet [37], VMUNet v2 [57], H-vmunet [50], UltraLight-VM-UNet [51], and SkinMamba. Tab. 1 and Tab. 2 show the comparative results on the ISIC2017 and ISIC2018 datasets, respectively. Our proposed SkinMamba outperformed the other models in terms of mIoU, DSC, Acc, Spe, and Sen metrics.

4.5   Ablation Experiment

We conducted comprehensive ablation experiments on the ISIC2018 dataset to validate the effectiveness of each component in our proposed model. These experiments included evaluating the performance of VSSB, SRSSB, and FBGM components.

Table 4: Quantitative comparisons with different combinations of the FBGM and SRSSB.

Ver.	FBGM	SRSSB	mIoU(%)↑	DSC(%)↑	Acc(%)↑
Ver 1			77.90	87.58	93.84
Ver 2		✓	79.90	88.83	94.60
Ver 3	✓		78.20	87.77	94.16
Ver 4	✓	✓	80.65	89.29	94.73

Effects of Visual State Space Block. We first analyzed the performance of CNN, Transformer, and Mamba within the framework. Specifically, we replaced the VSSB with 3×3 convolutions from CNN and self-attention mechanisms from Transformer. As shown in Tab. 3, replacing VSSB with convolutions or self-attention resulted in a decrease in performance.

Effects of Key Components. To further demonstrate the effectiveness of key components in SkinMamba, we performed ablation experiments by progressively removing or replacing each component. These components include SRSSB and FBGM. As shown in Tab. 4, each component significantly contributed to the model's performance. Specifically, the introduction of FBGM improved boundary detection and provided strong guidance for the decoder, while SRSSB enhanced cross-scale feature representation in a global context. Removing these components led to a decrease in both model accuracy and segmentation quality.

5   Conclusions and Future Works

This study presents SkinMamba, an innovative skin lesion segmentation model that combines State Space Models (SSM) with Convolutional Neural Networks (CNN). By introducing the Scale Residual State Space Block (SRSSB) and the Frequency Boundary Guided Module (FBGM), SkinMamba effectively addresses the limitations of existing models in handling multi-scale lesion areas, boundary blurring, and Inconspicuous lesion regions. Extensive experiments on the ISIC2017 and ISIC2018 datasets demonstrate that SkinMamba outperforms current state-of-the-art methods in metrics such as mIoU, DSC, Acc, Spe, and Sen, showcasing its superior capability in accurately segmenting skin lesion areas. The success of SkinMamba is attributed to its complementary strengths in global and local feature extraction. SRSSB enables efficient global modeling, capturing cross-scale information, while FBGM enhances boundary detection by extracting boundary cues from the frequency domain.

Although SkinMamba has performed excellently in experiments, there is room for further optimization. Future research will focus on improving the model's adaptability and generalization, particularly in other medical image segmentation tasks. Additionally, we aim to reduce the model's complexity, ensuring that SkinMamba exhibits higher efficiency and adaptability on edge devices and

in resource-constrained environments, thus expanding its potential application in real-time medical diagnosis systems.

References

1. Aghdam, E.K., Azad, R., Zarvani, M., Merhof, D.: Attention swin u-net: Cross-contextual attention mechanism for skin lesion segmentation. In: 2023 IEEE 20th International Symposium on Biomedical Imaging (ISBI). pp. 1–5. IEEE (2023). https://doi.org/10.1109/ISBI53787.2023.10230337 4, 10, 11

2. Alom, M.Z., Hasan, M., Yakopcic, C., Taha, T.M., Asari, V.K.: Recurrent residual convolutional neural network based on u-net (r2u-net) for medical image segmentation. arXiv preprint arXiv:1802.06955 (2018). https://doi.org/10.48550/arXiv.1802.06955 10, 11

3. Azad, R., Aghdam, E.K., Rauland, A., Jia, Y., Avval, A.H., Bozorgpour, A., Karimijafarbigloo, S., Cohen, J.P., Adeli, E., Merhof, D.: Medical image segmentation review: The success of u-net. IEEE Transactions on Pattern Analysis and Machine Intelligence (2024). https://doi.org/10.1109/TPAMI.2024.3435571 2

4. Cao, H., Wang, Y., Chen, J., Jiang, D., Zhang, X., Tian, Q., Wang, M.: Swin-unet: Unet-like pure transformer for medical image segmentation. In: Proceedings of the European Conference on Computer Vision Workshops(ECCVW) (2022). https://doi.org/10.1007/978-3-031-25066-8_9 4

5. Chan, H.P., Hadjiiski, L.M., Samala, R.K.: Computer-aided diagnosis in the era of deep learning. Medical physics **47**(5), e218–e227 (2020). https://doi.org/10.1002/mp.13764 2

6. Chen, H., Song, J., Han, C., Xia, J., Yokoya, N.: Changemamba: Remote sensing change detection with spatiotemporal state space model. IEEE Transactions on Geoscience and Remote Sensing **62**, 1–20 (2024). https://doi.org/10.1109/TGRS.2024.3417253 4

7. Chen, J., Mei, J., Li, X., Lu, Y., Yu, Q., Wei, Q., Luo, X., Xie, Y., Adeli, E., Wang, Y., et al.: Transunet: Rethinking the u-net architecture design for medical image segmentation through the lens of transformers. Medical Image Analysis p. 103280 (2024). https://doi.org/10.1016/j.media.2024.103280 4

8. Chen, Z., Ge, Y.: Mambauie&sr: Unraveling the ocean's secrets with only 2.8 flops. arXiv preprint arXiv:2404.13884 (2024). https://doi.org/10.48550/arXiv.2404.13884 4

9. Codella, N., Rotemberg, V., Tschandl, P., Celebi, M.E., Dusza, S., Gutman, D., Helba, B., Kalloo, A., Liopyris, K., Marchetti, M., et al.: Skin lesion analysis toward melanoma detection 2018: A challenge hosted by the international skin imaging collaboration (isic). arXiv preprint arXiv:1902.03368 (2019). https://doi.org/10.48550/arXiv.1902.03368 9

10. Codella, N.C.F., Gutman, D., Celebi, M.E., Helba, B., Marchetti, M.A., Dusza, S.W., Kalloo, A., Liopyris, K., Mishra, N., Kittler, H., Halpern, A.: Skin lesion analysis toward melanoma detection: A challenge at the 2017 international symposium on biomedical imaging (isbi), hosted by the international skin imaging collaboration (isic). In: 2018 IEEE 15th International Symposium on Biomedical Imaging (ISBI 2018). pp. 168–172 (2018). https://doi.org/10.1109/ISBI.2018.8363547 9

11. Dao, T., Gu, A.: Transformers are SSMs: Generalized models and efficient algorithms through structured state space duality. In: International Conference on Machine Learning (ICML) (2024). https://doi.org/10.48550/arXiv.2405.21060 2

12. Dosovitskiy, A., Beyer, L., Kolesnikov, A., Weissenborn, D., Zhai, X., Unterthiner, T., Dehghani, M., Minderer, M., Heigold, G., Gelly, S., Uszkoreit, J., Houlsby, N.: An image is worth 16x16 words: Transformers for image recognition at scale. ICLR (2021). https://doi.org/10.48550/arXiv.2010.11929 9

13. Fu, D.Y., Dao, T., Saab, K.K., Thomas, A.W., Rudra, A., Ré, C.: Hungry Hungry Hippos: Towards language modeling with state space models. In: International Conference on Learning Representations (2023). https://doi.org/10.48550/arXiv.2212.14052 2

14. Ge, Y., Chen, Z., Yu, M., Yue, Q., You, R., Zhu, L.: Mambatsr: You only need 90k parameters for traffic sign recognition. Neurocomputing **599**, 128104 (2024). https://doi.org/10.1016/j.neucom.2024.128104 4

15. Gu, A., Goel, K., Re, C.: Efficiently modeling long sequences with structured state spaces. In: International Conference on Learning Representations (2022), 10.48550/arXiv.2111.00396 2, 4

16. Gu, A., Johnson, I., Goel, K., Saab, K.K., Dao, T., Rudra, A., R'e, C.: Combining recurrent, convolutional, and continuous-time models with linear state-space layers. In: Neural Information Processing Systems (2021). https://doi.org/10.48550/arXiv.2110.13985 4

17. Guan, S., Khan, A.A., Sikdar, S., Chitnis, P.V.: Fully dense unet for 2-d sparse photoacoustic tomography artifact removal. IEEE Journal of Biomedical and Health Informatics **24**(2), 568–576 (2020). https://doi.org/10.1109/JBHI.2019.2912935 3

18. Guo, H., Li, J., Dai, T., Ouyang, Z., Ren, X., Xia, S.T.: Mambair: A simple baseline for image restoration with state-space model. arXiv preprint arXiv:2402.15648 (2024). https://doi.org/10.48550/arXiv.2402.15648 4

19. Gupta, A., Gu, A., Berant, J.: Diagonal state spaces are as effective as structured state spaces. Advances in Neural Information Processing Systems **35**, 22982–22994 (2022). https://doi.org/10.48550/arXiv.2203.14343 2

20. Hadjiiski, L., Cha, K., Chan, H.P., Drukker, K., Morra, L., Näppi, J.J., Sahiner, B., Yoshida, H., Chen, Q., Deserno, T.M., et al.: Aapm task group report 273: recommendations on best practices for ai and machine learning for computer-aided diagnosis in medical imaging. Medical Physics **50**(2), e1–e24 (2023). https://doi.org/10.1002/mp.16188 2

21. Hao, J., He, L., Hung, K.F.: T-mamba: Frequency-enhanced gated long-range dependency for tooth 3d cbct segmentation. arXiv preprint arXiv:2404.01065 (2024). https://doi.org/10.48550/arXiv.2404.01065 4

22. He, A., Wang, K., Li, T., Du, C., Xia, S., Fu, H.: H2former: An efficient hierarchical hybrid transformer for medical image segmentation. IEEE Transactions on Medical Imaging **42**(9), 2763–2775 (2023). https://doi.org/10.1109/TMI.2023.3264513 10, 11

23. Huang, X., Deng, Z., Li, D., Yuan, X., Fu, Y.: Missformer: An effective transformer for 2d medical image segmentation. IEEE Transactions on Medical Imaging **42**(5), 1484–1494 (2023). https://doi.org/10.1109/TMI.2022.3230943 10, 11

24. Kalman, R.E.: A new approach to linear filtering and prediction problems. Journal of Basic Engineering (1960). https://doi.org/10.1002/mp.13764 2, 4

25. Leming, M.J., Bron, E.E., Bruffaerts, R., Ou, Y., Iglesias, J.E., Gollub, R.L., Im, H.: Challenges of implementing computer-aided diagnostic models for neuroimages in a clinical setting. NPJ Digital Medicine **6**(1), 129 (2023). https://doi.org/10.1038/s41746-023-00868-x 2

26. Liang, D., Zhou, X., Wang, X., Zhu, X., Xu, W., Zou, Z., Ye, X., Bai, X.: Point-mamba: A simple state space model for point cloud analysis. arXiv preprint arXiv:2402.10739 (2024). https://doi.org/10.48550/arXiv.2402.10739 4

27. Lin, W.S., Wu, Z., Chen, J., Huang, J., Jin, L.: Scale-aware modulation meet transformer. 2023 IEEE/CVF International Conference on Computer Vision (ICCV) pp. 5992–6003 (2023). https://doi.org/10.1109/ICCV51070.2023.00553 2

28. Liu, Y., Tian, Y., Zhao, Y., Yu, H., Xie, L., Wang, Y., Ye, Q., Liu, Y.: Vmamba: Visual state space model. arXiv preprint arXiv:2401.10166 (2024). https://doi.org/10.48550/arXiv.2401.10166 2, 4

29. Liu, Z., Lin, Y., Cao, Y., Hu, H., Wei, Y., Zhang, Z., Lin, S., Guo, B.: Swin transformer: Hierarchical vision transformer using shifted windows. In: Proceedings of the IEEE/CVF International Conference on Computer Vision (ICCV) (2021). https://doi.org/10.1109/ICCV48922.2021.00986 2

30. Long, J., Shelhamer, E., Darrell, T.: Fully convolutional networks for semantic segmentation. In: Proceedings of the IEEE conference on computer vision and pattern recognition. pp. 3431–3440 (2015). https://doi.org/10.1109/TPAMI.2016.2572683 3

31. Ma, J., Li, F., Wang, B.: U-mamba: Enhancing long-range dependency for biomedical image segmentation. ArXiv abs/2401.04722 (2024). https://doi.org/10.48550/arXiv.2401.04722 2, 4

32. Mehta, H., Gupta, A., Cutkosky, A., Neyshabur, B.: Long range language modeling via gated state spaces. ArXiv abs/2206.13947 (2022). https://doi.org/10.48550/arXiv.2206.13947 4

33. Oktay, O., Schlemper, J., Folgoc, L.L., Lee, M., Heinrich, M., Misawa, K., Mori, K., McDonagh, S., Hammerla, N.Y., Kainz, B., et al.: Attention u-net: Learning where to look for the pancreas. arXiv preprint arXiv:1804.03999 (2018). https://doi.org/10.48550/arXiv.1804.03999 3

34. Peng, Y., Sonka, M., Chen, D.Z.: U-net v2: Rethinking the skip connections of u-net for medical image segmentation. arXiv preprint arXiv:2311.17791 (2023). https://doi.org/10.48550/arXiv.2311.17791 3

35. Rahman, M.M., Marculescu, R.: Medical image segmentation via cascaded attention decoding. In: Proceedings of the IEEE/CVF Winter Conference on Applications of Computer Vision. pp. 6222–6231 (2023). https://doi.org/10.1109/WACV56688.2023.00616 2

36. Ronneberger, O., Fischer, P., Brox, T.: U-net: Convolutional networks for biomedical image segmentation. In: Medical image computing and computer-assisted intervention–MICCAI 2015: 18th international conference, Munich, Germany, October 5-9, 2015, proceedings, part III 18. pp. 234–241. Springer (2015). https://doi.org/10.1007/978-3-319-24574-4_28 3, 10, 11

37. Ruan, J., Xiang, S.: Vm-unet: Vision mamba unet for medical image segmentation. ArXiv abs/2402.02491 (2024). https://doi.org/10.48550/arXiv.2402.02491 2, 4, 10, 11

38. Ruan, J., Xiang, S., Xie, M., Liu, T., Fu, Y.: Malunet: A multi-attention and lightweight unet for skin lesion segmentation. In: 2022 IEEE International Conference on Bioinformatics and Biomedicine (BIBM). pp. 1150–1156. IEEE (2022). https://doi.org/10.1109/BIBM55620.2022.9995040 9, 10, 11

39. Ruan, J., Xie, M., Gao, J., Liu, T., Fu, Y.: Ege-unet: an efficient group enhanced unet for skin lesion segmentation. In: International conference on medical image computing and computer-assisted intervention. pp. 481–490. Springer (2023). https://doi.org/10.1007/978-3-031-43901-8_46 9, 10, 11

40. Shi, Y., Xia, B., Jin, X., Wang, X., Zhao, T., Xia, X., Xiao, X., Yang, W.: Vmambair: Visual state space model for image restoration. arXiv preprint arXiv:2403.11423 (2024). https://doi.org/10.48550/arXiv.2403.11423 4

41. Siegel, R.L., Miller, K.D., Wagle, N.S., Jemal, A.: Cancer statistics, 2023. CA: a cancer journal for clinicians **73**(1) (2023). https://doi.org/10.3322/caac.21763 2

42. Smith, J.T., Warrington, A., Linderman, S.: Simplified state space layers for sequence modeling. In: The Eleventh International Conference on Learning Representations (2023). https://doi.org/10.48550/arXiv.2208.04933 4

43. Tang, C., Ji, J., Tang, Y., Gao, S., Tang, Z., Todo, Y.: A novel machine learning technique for computer-aided diagnosis. Engineering Applications of Artificial Intelligence **92**, 103627 (2020). https://doi.org/10.1016/j.engappai.2020.103627 2

44. Touvron, H., Cord, M., Douze, M., Massa, F., Sablayrolles, A., J'egou, H.: Training data-efficient image transformers & distillation through attention. In: International Conference on Machine Learning (2020). https://doi.org/10.48550/arXiv.2012.128771 2

45. Tu, Z., Talebi, H., Zhang, H., Yang, F., Milanfar, P., Bovik, A., Li, Y.: Maxvit: Multi-axis vision transformer. ECCV (2022). https://doi.org/10.1007/978-3-031-20053-3_27 2

46. Vaswani, A.: Attention is all you need. Advances in Neural Information Processing Systems (2017). https://doi.org/10.48550/arXiv.1706.03762 3, 4

47. Wang, W., Xie, E., Li, X., Fan, D.P., Song, K., Liang, D., Lu, T., Luo, P., Shao, L.: Pyramid vision transformer: A versatile backbone for dense prediction without convolutions. In: 2021 IEEE/CVF International Conference on Computer Vision (ICCV). pp. 548–558 (2021). https://doi.org/10.1109/ICCV48922.2021.00061 2

48. Wu, J., Ji, W., Fu, H., Xu, M., Jin, Y., Xu, Y.: Medsegdiff-v2: Diffusion-based medical image segmentation with transformer. In: Proceedings of the AAAI Conference on Artificial Intelligence. vol. 38, pp. 6030–6038 (2024). https://doi.org/10.1609/aaai.v38i6.28418 2

49. Wu, R., Liang, P., Huang, X., Shi, L., Gu, Y., Zhu, H., Chang, Q.: Mhorunet: High-order spatial interaction unet for skin lesion segmentation. Biomedical Signal Processing and Control **88**, 105517 (2024). https://doi.org/10.1016/j.bspc.2023.105517 10, 11

50. Wu, R., Liu, Y., Liang, P., Chang, Q.: H-vmunet: High-order vision mamba unet for medical image segmentation. arXiv preprint arXiv:2403.13642 (2024). https://doi.org/10.48550/arXiv.2403.13642 2, 10, 11

51. Wu, R., Liu, Y., Liang, P., Chang, Q.: Ultralight vm-unet: Parallel vision mamba significantly reduces parameters for skin lesion segmentation. arXiv preprint arXiv:2403.20035 (2024). https://doi.org/10.48550/arXiv.2403.20035 10, 11

52. Xiao, H., Li, L., Liu, Q., Zhu, X., Zhang, Q.: Transformers in medical image segmentation: A review. Biomedical Signal Processing and Control **84**, 104791 (2023). https://doi.org/10.1016/j.bspc.2023.104791 2

53. Xiao, X., Lian, S., Luo, Z., Li, S.: Weighted res-unet for high-quality retina vessel segmentation. In: 2018 9th International Conference on Information Technology in Medicine and Education (ITME). pp. 327–331 (2018). https://doi.org/10.1109/ITME.2018.00080 3

54. Xing, Z., Ye, T., Yang, Y., Liu, G., Zhu, L.: Segmamba: Long-range sequential modeling mamba for 3d medical image segmentation. arXiv preprint arXiv:2401.13560 (2024). https://doi.org/10.48550/arXiv.2401.13560 4

55. Yang, G., Du, K., Yang, Z., Du, Y., Zheng, Y., Wang, S.: Cmvim: Contrastive masked vim autoencoder for 3d multi-modal representation learning for ad classification. arXiv preprint arXiv:2403.16520 (2024). https://doi.org/10.48550/arXiv.2403.16520 4

56. Yuan, F., Zhang, Z., Fang, Z.: An effective cnn and transformer complementary network for medical image segmentation. Pattern Recognition 136, 109228 (2023). https://doi.org/10.1016/j.patcog.2022.109228 2

57. Zhang, M., Yu, Y., Jin, S., Gu, L., Ling, T., Tao, X.: Vm-unet-v2: rethinking vision mamba unet for medical image segmentation. In: International Symposium on Bioinformatics Research and Applications. pp. 335–346. Springer (2024). https://doi.org/10.1007/978-981-97-5128-0_27 10, 11

58. Zhang, T., Li, X., Yuan, H., Ji, S., Yan, S.: Point could mamba: Point cloud learning via state space model. arXiv preprint arXiv:2403.00762 (2024). https://doi.org/10.48550/arXiv.2403.00762 4

59. Zhao, S., Chen, H., Zhang, X., Xiao, P., Bai, L., Ouyang, W.: Rs-mamba for large remote sensing image dense prediction. IEEE Transactions on Geoscience and Remote Sensing 62, 1–14 (2024). https://doi.org/10.1109/TGRS.2024.3425540 4

60. Zheng, Z., Wu, C.: U-shaped vision mamba for single image dehazing. arXiv preprint arXiv:2402.04139 (2024). https://doi.org/10.48550/arXiv.2402.04139 4

61. Zhou, H.Y., Guo, J., Zhang, Y., Han, X., Yu, L., Wang, L., Yu, Y.: nnformer: Volumetric medical image segmentation via a 3d transformer. IEEE Transactions on Image Processing (2023). https://doi.org/10.1109/TIP.2023.3293771 2

62. Zhou, Z., Siddiquee, M.M.R., Tajbakhsh, N., Liang, J.: Unet++: Redesigning skip connections to exploit multiscale features in image segmentation. IEEE Transactions on Medical Imaging (2019). https://doi.org/10.1109/TMI.2019.2959609 3, 10, 11

63. Zhu, L., Liao, B., Zhang, Q., Wang, X., Liu, W., Wang, X.: Vision mamba: Efficient visual representation learning with bidirectional state space model. arXiv preprint arXiv:2401.09417 (2024). https://doi.org/10.48550/arXiv.2401.09417 2

64. Zhu, Q., Cai, Y., Fang, Y., Yang, Y., Chen, C., Fan, L., Nguyen, A.: Samba: Semantic segmentation of remotely sensed images with state space model. arXiv preprint arXiv:2404.01705 (2024). https://doi.org/10.48550/arXiv.2404.01705 4

65. Zou, S., Zhang, Z., Gao, G.: Octamamba: A state-space model approach for precision octa vasculature segmentation. arXiv preprint arXiv:2409.08000 (2024). https://doi.org/10.48550/arXiv.2409.08000 2

66. Zou, S., Zhang, Z., Zou, Y., Gao, G.: Microscopic-mamba: Revealing the secrets of microscopic images with just 4m parameters. arXiv preprint arXiv:2409.07896 (2024). https://doi.org/10.48550/arXiv.2409.07896 4

67. Zuo, Q., Chen, S., Wang, Z., Zhang, L.: R2au-net: Attention recurrent residual convolutional neural network for multimodal medical image segmentation. Sec. and Commun. Netw. 2021 (jan 2021). https://doi.org/10.1155/2021/6625688 10, 11